Journal of Molecular Catalysis A: Chemical 300 (2009) 72–79

Contents lists available at ScienceDirect

Journal of Molecular Catalysis A: Chemical

journal homepage: www.elsevier.com/locate/molcata

Exposed crystal surface-controlled TiO_2 nanorods having rutile phase from $TiCl_3$ under hydrothermal conditions

Eunyoung Bae, Naoya Murakami, Teruhisa Ohno*

Department of Materials Science, Faculty of Engineering, Kyushu Institute of Technology, 1-1 Sensuicho, Tobata-ku, Kitakyushu 804-8550, Japan

ARTICLE INFO

Article history:
Received 4 July 2008
Received in revised form 14 October 2008
Accepted 19 October 2008
Available online 8 November 2008

Keywords:
Photocatalyst
Exposed crystal surface
Rutile crystal phase
Separation of reaction site
Improvement of charge separation

ABSTRACT

Size-, shape-, and phase structure-controlled synthesis of TiO_2 nanocrystallites has long been one of the main themes in TiO_2 research. Many synthetic techniques have been utilized in the preparation of TiO_2 nanocrystals, among which hydrothermal treatment has been drawing much attention because it directly produces well-crystallized nanocrystallities of a wide range of compositions of crystal phases within a short reaction time. In this study, we carried out hydrothermal growth of rutile TiO_2 rods by using aqueous titanium trichloride ($TiCl_3$) solutions containing NaCl. Uniform ultrafine rutile TiO_2 particles were obtained, and developed crystal faces were observed by TEM, SEM, XRD, and specific surface area measurements. The obtained rutile fine particles showed high levels of activity for degradation of 2-propanol and acetaldehyde under UV irradiation compared to the activity levels of anatase fine particles (ST-01) developed for environmental clean-up. The surface chemistry of the rutile TiO_2 particles was also investigated. From photodeposition of Pt and PbO_2, we suggest that the (1 1 0) face provides reductive sites and that the (1 1 1) face provides oxidative sites. These results indicate that the crystal faces facilitate the separation of electrons and holes, resulting in improvement of photocatalytic activity.

1. Introduction

TiO_2 photocatalysis has been intensively investigated for environmental remediation and energy conversion [1–5]. Because the efficiency of TiO_2 photocatalytic reactions is largely determined by interfacial charge transfers, various surface modification methods have been developed to facilitate the charge transfer. TiO_2 exists in three crystal structures: rutile, anatase and brookite. Each crystalline structure exhibits specific physical properties, band gap, surface states, etc. [6]. Rutile TiO_2 has some advantages over anatase such as higher chemical stability and higher refractive index. It is of fundamental significance to explore mild synthetic techniques by which particle shapes, nano- and micro-meter-scale morphologies, and crystallinity are well defined and controlled [7–9]. Moreover, surface chemistry of single-crystalline rutile particles has been the subject of intensive studies because their chemical activity depends greatly on surface structures [10].

TiO_2 can be prepared by various methods, including sol–gel [11], hydrothermal [10,12–14], combustion synthesis [15], and gas-phase [16,17] methods. Much attention has been paid to the hydrothermal method because of its high productivity and convenience. In general, the hydrothermal method is carried out by changing the physicochemical parameters of the system, such as temperature, pH, and concentration of reactants. Recently, it has been reported that rutile TiO_2 nanoparticles could be uniformly coated on the surface of glass using $TiCl_3$ and NaCl as starting materials by the hydrothermal method [7,18].

Photocatalytic reaction on TiO_2 is induced by excited electrons and positive holes. However, recombination may occur on the surface or in the bulk, which is promoted by impurities or defects. All factors are introduced into the crystal by generation of bulk or surface imperfections [19]. Well-crystallized faceted particles showed enhanced photocatalytic activity compared to powders with poorly crystalline surface and the photocatalytic activity increased with increase in crystallite size, the surface itself being an intrinsic defect [20]. All of the TiO_2 nanorods investigated in the present study were well-crystallized and well-faceted as a consequence of the ripening processes occurring under hydrothermal conditions.

It has been shown that individual crystal faces on TiO_2 particles play an important role [21]. The importance of the crystal faces of photocatalyst particles should be related to the fact that oxidation and reduction occur simultaneously on each particle. Because of their different atomic arrangements, the presence of well-developed faces on TiO_2 nanorods is favorable for providing both oxidation and reduction sites [22]. It is also expected that the efficiency of electron–hole separation is enhanced due to the difference in energy levels between different crystal faces. Ohno et al.

* Corresponding author. Tel.: +81 93 884 3318; fax: +81 93 884 3318.
E-mail address: tohno@che.kyutech.ac.jp (T. Ohno).

1381-1169/$ – see front matter © 2008 Elsevier B.V. All rights reserved.
doi:10.1016/j.molcata.2008.10.048

focused on rutile TiO_2 rods in a mixture of anatase and rutile particles provided by Toho Co. Ltd., Japan and have demonstrated that the (1 1 0) face provides reductive sites and that the (0 1 1) face provides oxidative sites [23]. Here, we report that each crystal face of rutile TiO_2 provides reduction and oxidation sites. This suggests that rutile TiO_2 nanorods should have higher spatial separation between oxidation and reduction sites with lower probability of recombination.

We report here the results of an extensive investigation on the hydrothermal synthesis of TiO_2 using aqueous $TiCl_3$ and NaCl as reactants. The resulting products were fully characterized, and the effects of temperature and reaction time on crystallinity, crystal size, and crystal shape were determined. The photocatalytic activities of the different samples in the oxidation of acetaldehyde and 2-propanol were determined and were found to be correlated with crystallinity and crystal shape of the rutile TiO_2 nanorods. We demonstrate that the crystal surface structure of TiO_2 nanorods can be controlled by adjusting the concentration of NaCl and reaction time. These TiO_2 nanorods are expected to show high levels of photocatalytic activity due to the different crystal faces.

2. Experimental

2.1. Chemicals

All chemical reagents were commercial products used without further treatment. Titanium trichloride ($TiCl_3$), sodium chloride (NaCl), 2-propanol ($(CH_3)_2CHOH$), hexachloroplatinic acid ($H_2PtCl_6{\cdot}6H_2O$), lead nitrate ($Pb(NO_3)_2$), and nitric acid (HNO_3) were purchased from Wako (all of reagent grade), and acetaldehyde (CH_3CHO) was purchased from Aldrich. TiO_2 (ST-01, Ishihara), an anatase with an average surface area of 300 $m^2\,g^{-1}$, and TiO_2 (MT-600B, Tayca), a rutile with an average surface area of 25–35 $m^2\,g^{-1}$, were used as reference photocatalysts.

2.2. Synthesis of TiO_2

In a typical synthesis procedure, a chemical solution was put in a sealed Teflon-lined autoclave reactor containing 50 ml aqueous solution of titanium trichloride ($TiCl_3$, 0.15 M) and sodium chloride (NaCl, 1 M, 3 M and 5 M). The solutions were then put into a 200 °C oven for 3 or 6 h. The substrate was centrifuged and rinsed with deionized water and then dried in a vacuum oven. Throughout this paper, samples are referred to as SH1 (NaCl 1 M), SH3 (NaCl 3 M) and SH5 (NaCl 5 M).

2.3. Photocatalytic deposition of Pt and PbO_2 on TiO_2 powder

For Pt/TiO_2 preparation, an aqueous TiO_2 suspension (SH3) (2 g/L) containing 0.52 M 2-propanol and 1 mM hexachloroplatinic acid ($H_2PtCl_6{\cdot}6H_2O$) was irradiated with a 300 W mercury UV lamp (Wacom Model XDS-501S) for 24 h. N_2 gas was purged through the suspension prior to UV irradiation to remove oxygen. The light intensity was about 1 mW cm^{-2}. After irradiation, the color of the powder changed from white to silver, and the suspension was centrifuged and washed with distilled water and then collected as powder after drying at 70 °C under reduced pressure for 3 h.

Using this platinized TiO_2 powder, Pb^{2+} ions were oxidized into PbO_2. This reaction was carried out in an aqueous Pt/TiO_2 suspension (2 g/L) containing 0.1 M $Pb(NO_3)_2$ under aerated conditions. The pH of the solution for this reaction was adjusted to 1.0 by the addition of nitric acid according to the literature [23,24]. After photoreaction using a 500 W Hg lamp (Ushio Co. Ltd., SX-UI501HQ) for 24 h, the color of the powder changed from silver to brown, indicating that PbO_2 had been deposited on the surface. The light intensity was about 0.1 W cm^{-2}. Pt and PbO_2 particles deposited on TiO_2 were observed in SEM, EDX and TEM images.

2.4. Characterization

Phase identification was performed via X-ray diffraction (XRD) with Cu Kα radiation. The mean grain size was determined from Scherrer's equation. The morphology of the samples was observed by field emission scanning electron microscopy (FE-SEM) and transmission electron microscopy (TEM). The specific surface area was determined by using the Brunauer–Emmett–Teller method [25].

2.5. Photocatalytic activity test

The photocatalytic activities of the samples were evaluated by the degradation of 2-propanol in the liquid phase and acetaldehyde in the gas phase. The photocatalytic generation of acetone by 5 g/L TiO_2 dispersed in 2-propanol (50 mM, in acetonitrile) was measured in a Pyrex test tube reactor. The TiO_2/2-propanol suspension was illuminated by a 300 W Xe lamp (Eagle LX 300). The light beam was passed through a UV-35 filter to cut off wavelength shorter than 350 nm. Fine stainless meshes were used as neutral density filters to adjust the irradiation intensity (150 mW cm^{-2}). During the reaction, the suspension was continuously stirred. Samples of the reaction mixture were centrifuged to remove TiO_2. The acetone content was analyzed on a gas chromatograph (Hitachi Model G-3500). Reference samples were selected to test the generality of our results and include ST-01 as anatase and MT-600B as rutile.

The photocatalytic activity of TiO_2 nanoparticles was evaluated by measuring the change in concentration of acetaldehyde and evolved CO_2 as a function of irradiation time. A Tedlar bag (As One Co. Ltd.) was used as the photoreactor vessel. One hundred mg of TiO_2 powder was spread on the bottom of a glass dish, and this was placed in the reaction vessel. Five hundred ppmv of acetaldehyde was prepared in the vessel by injection of saturated gas acetaldehyde. The irradiation was conducted at room temperature after equilibrium between the gas and adsorbed acetaldehyde had been reached. The light source was a 500 W Xe-lamp (Ushio Co. Ltd., SX-UI501XQ). The light beam was passed through a UV-35 filter to cut off wavelength shorter than 350 nm. Fine stainless meshes were used as neutral density filters to adjust the irradiation intensity (10 or 30 mW cm^{-2}). After starting the irradiation, the decrease in acetaldehyde concentration and evolved carbon dioxide concentration was measured using a gas chromatograph (Shimadzu Model GC-8A and GC 14A, FID detector).

3. Results and discussion

3.1. XRD patterns and specific surface area of rutile nanorods

Fig. 1 shows the XRD patterns of samples treated at 200 °C for 6 h. All of the diffraction peaks agree with those of TiO_2 in the rutile form and no other phases were detected. The intensity of diffraction peaks of the rutile TiO_2 becomes stronger with increase in NaCl concentration, indicating improvement in crystallinity of the rutile rod as shown in Fig. 1. The mean grain size was determined from Scherrer's equation. By applying Scherrer's formula to the rutile (1 1 0) diffraction peaks, the average crystallite sizes of the samples were found to be 66.0, 72.7 and 97.2 nm for samples SH1, SH3 and SH5, respectively (as shown in Table 1). These results indicate that the crystal sizes of the resulting rutile nanorods increased with increase in the concentration of NaCl. The specific surface areas of samples are shown in Table 1. The BET surface area was decreased with an increase in the concentration of NaCl. A similar tendency

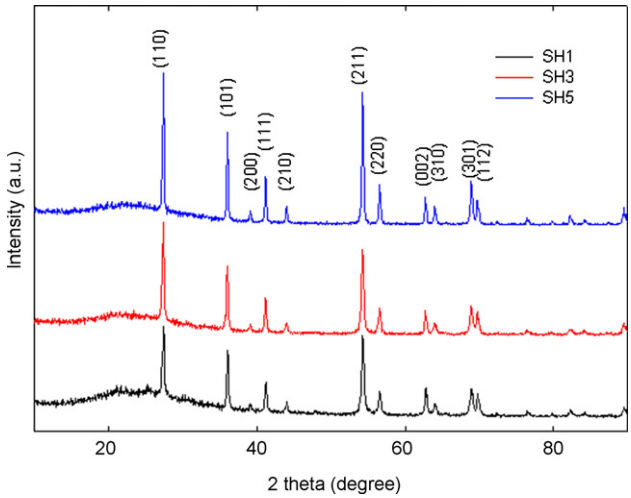

Fig. 1. XRD patterns of samples obtained from a $TiCl_3$ solution with various concentrations of NaCl after hydrothermal treatment for 6 h at 200 °C.

Table 1
Physical properties of rutile TiO_2 nanorod samples and reference TiO_2.

Sample	Synthesis conditions (M)		Mean crystallite size (nm)	BET surface area (m^2/g)
	$TiCl_3$	NaCl		
ST-01			7.0	300
MT-600B			50	25–35
SH1	0.15	1	65.95[a]	32.79
SH3	0.15	3	72.67[a]	25.94
SH5	0.15	5	97.20[a]	12.11

[a] Calculated as weighted mean value of the crystallite size (XRD) of TiO_2.

was observed for TiO_2 treated at 200 °C for 3 h (see Table 1S and Fig. 1S, Supporting Information, as an example). Furthermore, the crystal size of TiO_2 treated at 200 °C for 6 h was larger than that of TiO_2 treated at 200 °C for 3 h.

3.2. SEM observation of rutile nanorods

Fig. 2 shows SEM images of samples SH1, SH3 and SH5. Flower-like aggregation structures were observed in sample SH1 (Fig. 2a).

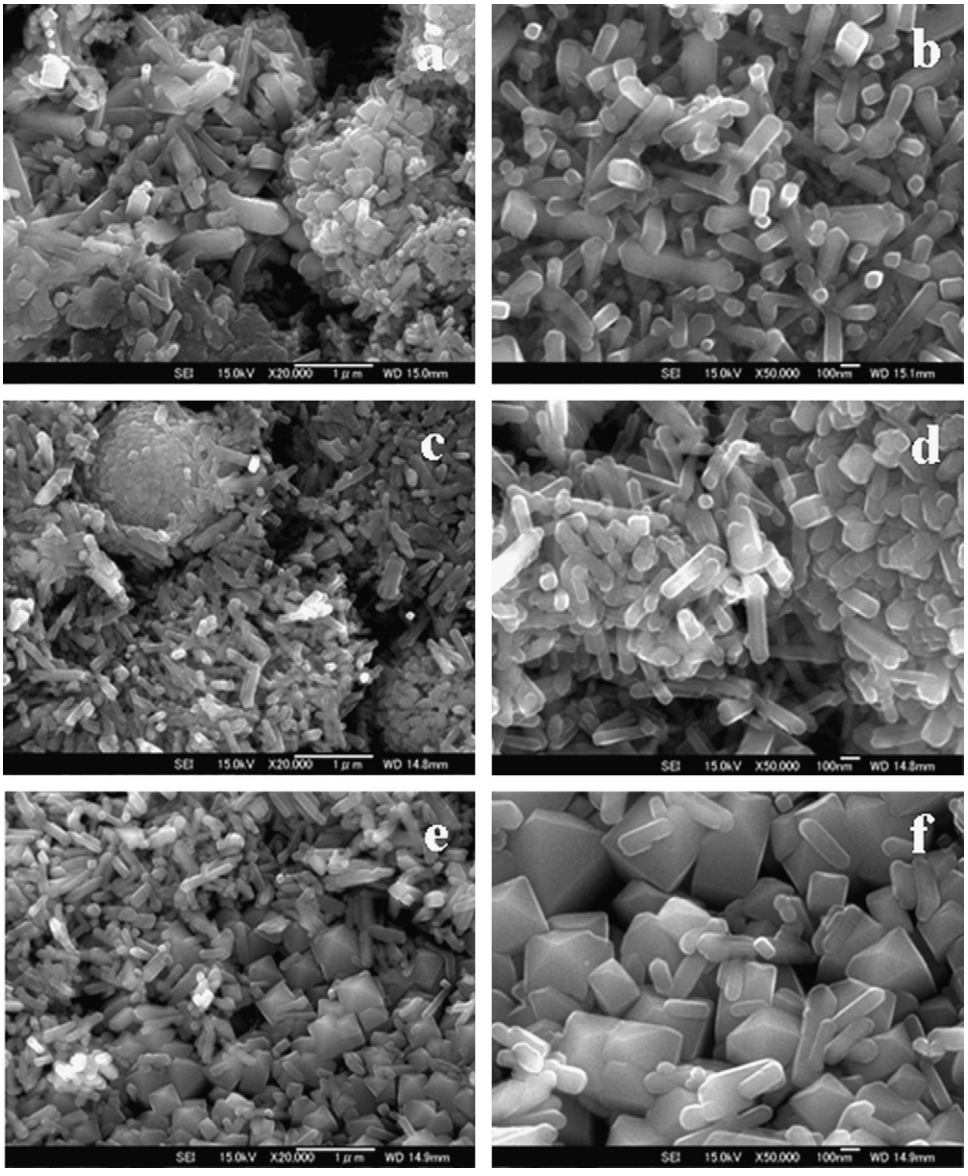

Fig. 2. SEM images of (a, b) SH1, (c, d) SH3 and (e, f) SH5.

Higher magnification revealed that these flower-like structures were composed of many nanorods with triangular tips. These nanorods were 60–100 nm in diameter and 300–400 nm in length (Fig. 2b). When the concentration of NaCl was increased from 1 M to 5 M, the aggregated nanorods dispersed and particle size increased (Fig. 2). The concentration of NaCl therefore played an important role in the growth of nanorods. When the concentration of NaCl was 1 M, most of the particles were agglomerated (Fig. 2a). When the concentration of NaCl was increased, the particles became larger and were well dispersed, as shown in Fig. 2. During hydrothermal treatment, rutile nanorods grew significantly with time. With a decrease in hydrothermal treatment time (3 h), the nanorods aggregated to form a flower-like structure as shown in Fig. S2 (Supporting information). Although the results of 3 h of treatment were similar to those of 6 h of treatment, the particle size and dispersion of nanorods were decreased after 3 h of treatment compared to those after 6 h of treatment. Therefore, NaCl is crucial for the formation and dispersion of rutile TiO_2 nanorods.

3.3. TEM and SAED observations of rutile nanorods

Fig. 3 shows TEM images and selected area electron diffraction (SAED) patterns taken from nanorods shown in TEM images in various conditions. TEM images showed the rod-like shape with a triangular end and tetragonal rutile structure and single-crystalline quality of the TiO_2 nanorod. TEM images (Fig. 3a, c and e) showed that the shape of end of the rod changed from a symmetric triangular tip to an asymmetric triangular tip when the concentration of NaCl was increased from 1 M to 5 M. The SAED patterns of the exposed surface of the end of the rod and side surface of the rod are assigned to (1 1 1) and (1 1 0), respectively. The growth of the TiO_2 rod occurs in the (0 0 1) direction. In addition, (0 0 1) crystal faces are exposed gradually with an increase in NaCl concentration. A spot pattern indicates a single-crystalline nature of the rutile TiO_2 nanorods. Fig. 3 shows that surface morphology of rutile TiO_2 is controlled by changing the concentration of NaCl.

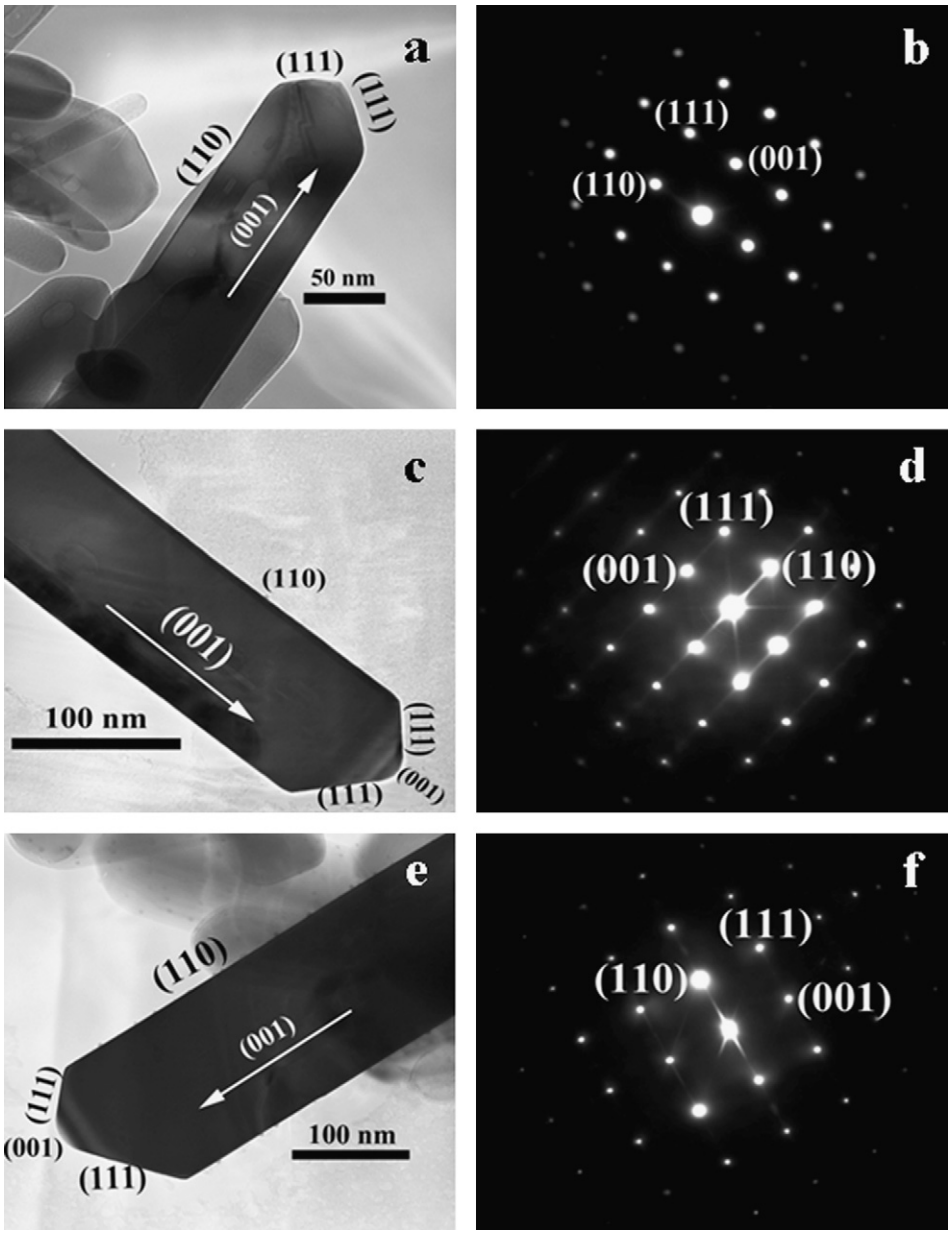

Fig. 3. TEM images (a, c, e) and SAED patterns (b, d, f). (a, b) SH1, (c, d) SH3 and (e, f) SH5.

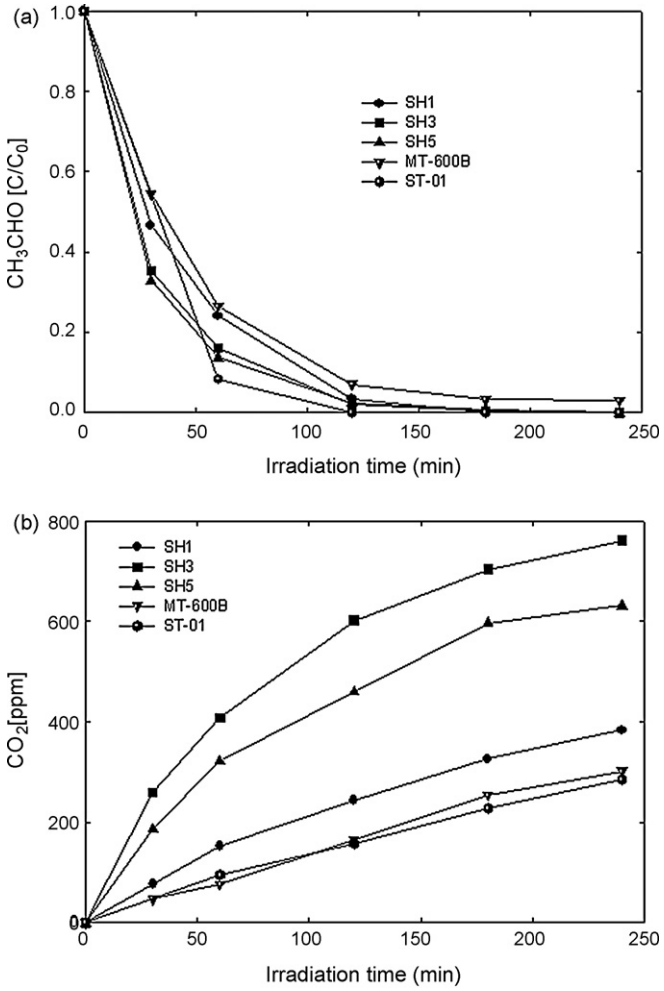

Fig. 4. Time profiles of decomposition of acetaldehyde on TiO_2 at different concentrations of NaCl at light intensity of 30 mW cm^{-2}. (a) Acetaldehyde, (b) CO_2. The experimental conditions were: [acetaldehyde]$_i$ = 500 ppm, [TiO_2] = 10.4 mg/cm^2, UV light (λ > 350 nm) irradiated.

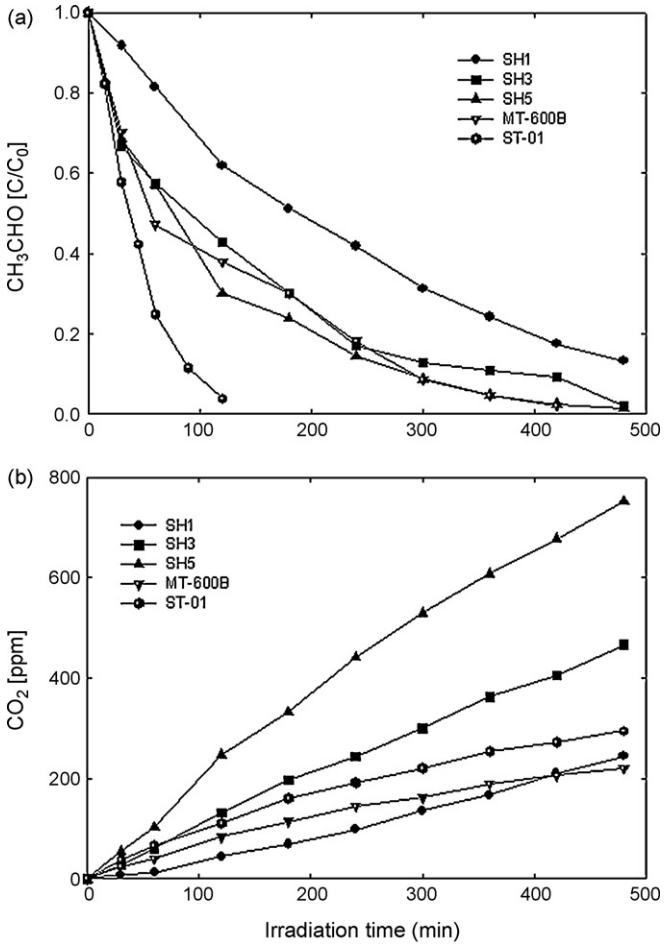

Fig. 5. Time profiles of decomposition of acetaldehyde on TiO_2 at different concentrations of NaCl at light intensity 10 mW cm^{-2}. (a) Acetaldehyde, (b) CO_2. The experimental conditions were: [acetaldehyde]$_i$ = 500 ppm, [TiO_2] = 10.4 mg/cm^2, UV light (λ > 350 nm) irradiated.

3.4. Photocatalytic activity

Fig. 4 shows photocatalytic evolution of CO_2 by decomposition of acetaldehyde on reference TiO_2 and SH1, SH3 and SH5 at light intensity of 30 mW cm^{-2}. Photocatalytic activity levels of rutile TiO_2 prepared by using NaCl are much higher than those of MT-600B and ST-01. The photocatalytic activity level of SH3 was the highest. These results suggested that the photocatalytic activity of the samples for acetaldehyde degradation is affected by exposed crystal surface of rutile TiO_2.

Fig. 5 shows photocatalytic evolution of CO_2 by decomposition of acetaldehyde on reference TiO_2 and SH1, SH3 and SH5 under the condition of low light intensity (10 mW cm^{-2}). Photocatalytic activity levels of rutile TiO_2 prepared using NaCl are higher than those of MT-600B and ST-01. SH5 showed the highest photocatalytic activity. The order of photocatalytic activities was SH3 > SH5 > SH1 > MT-600B > ST-01 in the case of high light intensity (as shown in Fig. 4b) and SH5 > SH3 > ST-01 > SH1 > MT-600B in the case of low light intensity (as shown in Fig. 5b).

According to the literature [26–28], it was assumed that reactions via two pathways occur: direct oxidation of acetaldehyde to evolve CO_2 (1) and evolution of CO_2 by oxidation of acetaldehyde via acetic acid, (2) and (3).

$$2CH_3CHO + 2OH^{\bullet} + O_2 \rightarrow 2CH^{\bullet}{}_3 + 2CO_2 + 2H_2O \quad (1)$$

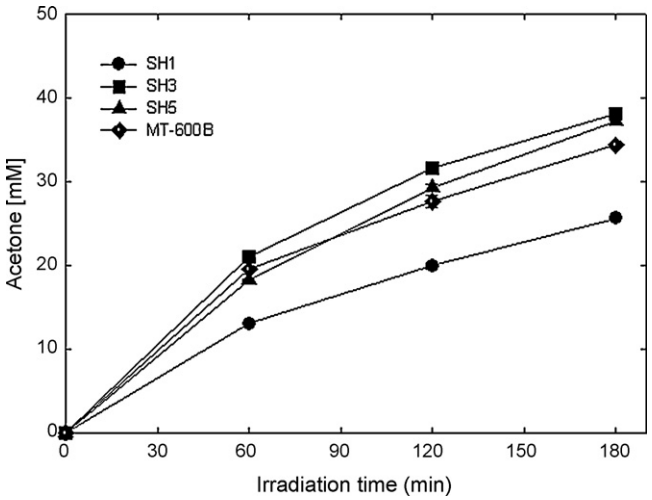

Fig. 6. Time profiles of decomposition of 2-propanol on TiO_2 at different concentrations of NaCl. The experimental conditions were: [2-propanol]$_i$ = 50 mM, [TiO_2] = 10 g/l, UV light (λ > 350 nm) irradiated (150 mW/cm^2).

$$CH_3CHO + OH^{\bullet} + O_2 \rightarrow CH_3COOH + HOO^{\bullet} \quad (2)$$

$$CH_3COOH + h^+ \rightarrow CO_2 + CH^{\bullet}{}_3 + H^+ \quad (3)$$

Fig. 4a and b shows photodegradation of acetaldehyde on TiO_2 photocatalysts under UV light irradiation with a light intensity of 30 mW cm^{-2}. After complete degradation of acetaldehyde in the gas phase, CO_2 was continuously evolved as shown in Fig. 4b. In addition, the rate of evolved CO_2 rapidly decreased in the case of SH3 and SH5 after complete disappearance of acetaldehyde in the gas phase (Fig. 4b). These results suggest that CO_2 was directly formed by the reaction between acetaldehyde and OH radicals according to route (1) at the initial stage of the reaction. After disappearance of acetaldehyde in the gas phase, CO_2 was evolved via acetic acid (route (2) and (3)) because oxidization of acetic acid is difficult compared to that of acetaldehyde. Therefore, the reaction rate of evolved CO_2 remarkably decreased after disappearance of acetaldehyde in the gas phase [26]. However, the rates of evolved CO_2 on SH1, ST-01 and MT-600B increased linearly even after complete disappearance of acetaldehyde. These results indicate that the evolution of CO_2 over SH1, ST-01 and MT-600B proceeded mainly via route (2) and (3) during photoirradiation.

Under weak photoirradiation with a light intensity of 10 mW cm^{-2}, the rate of CO_2 evolution increased linearly on all photocatalysts (MT-600B, ST-01, SH1, SH3, SH5) even after disappearance of acetaldehyde as shown in Fig. 5a and b. These results suggested that evolution of CO_2 may proceed via acetic acid (route

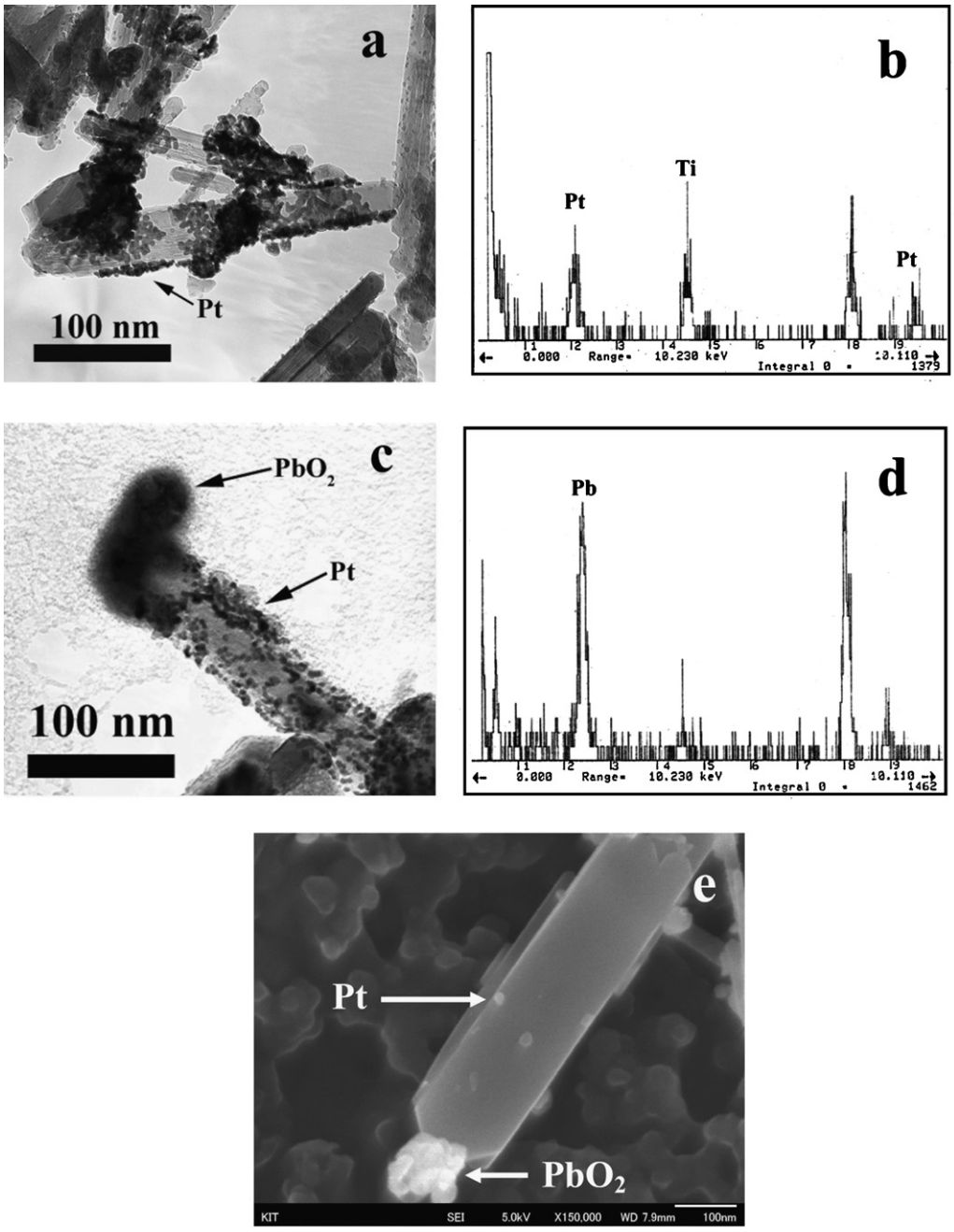

Fig. 7. TEM image (a) and EDX analysis (b) of rutile TiO_2 nanorod (SH3) on which Pt particles were deposited. TEM image (c), EDX analysis (d) and SEM image (e) of rutile TiO_2 nanorod (SH3) on which Pt and PbO_2 particles were deposited.

(2) and (3)). As mentioned above, the order of photocatalytic activity in the case of low light intensity is slightly different from that in the case of high light intensity.

Electron–hole pair production depends on irradiation intensity [29]. In illuminated semiconductor photocatalysts, charge-carrier (e^-, h^+) recombination and interfacial charge transfer are second- and first-order processes, respectively. The charge-carrier density increases with an increase in the absorbed light intensity. As a result, at a higher relative absorbed light intensity, the rate of charge-carrier recombination is increased compared with interfacial charge transfer. Therefore, quantum efficiency of reactions decreases with an increase in light intensity [30]. However, the relationship between the rate of charge-carrier recombination with incident light intensity and improvement of photocatalytic activity by separation of reaction sites of rutile fine particles (SH1, SH3, SH5) is not clear. This relationship will be discussed in another paper.

Fig. 6 shows photo-oxidation of 2-propanol. Acetone is the dominant intermediate product. Photocatalytic activity levels of TiO_2 nanorods are higher than those of MT-600B as a reference TiO_2, except for degradation of 2-propanol of SH1. The order of photocatalytic activities was SH3 > SH5 > MT-600B > SH1 in the case of 2-propanol. Among the photocatalysts used in this study, SH3 was the most active. This result is the same as the order of photocatalytic activity of acetaldehyde under the condition of high light intensity.

In these cases, it was observed that an increase in particle size led to an increase in activity except for reference TiO_2 (as shown in Table 1). As shown in Figs. 4–6, a decrease in surface area resulting from crystal growth did not cause a decrease in photocatalytic activity, indicating that the photodegradation process is not affected by surface properties of photocatalysts. However, control of exposed crystal surfaces of rutile nanorods is also one of the important factors for improving photocatalytic activity of TiO_2.

The large specific surface areas and small crystal sizes as well as high crystallinity of TiO_2 might usually play important roles in the enhancement of photocatalytic activities. However, separation of reaction sites on the photocatalyst particle by the exposed crystal surface of the rutile nanorod is a more important factor for improvement of photocatalytic activity because a rutile nanorod having a small surface area (10–30 $m^2\,g^{-1}$) showed a higher level of photocatalytic activity than ST-01 having a large surface area (300 $m^2\,g^{-1}$). These results indicate that the charge separation between photoexcited electrons and holes should be improved by optimization of the exposed crystal surfaces for reactions resulting in an increase in the photocatalytic activity.

3.5. Photocatalytic deposition of Pt and PbO_2 on TiO_2 nanorods

In order to clarify the photocatalytic reaction mechanism, it is important to identify the actual reactive sites of TiO_2 particles. It has been reported that oxidation and reduction sites on rutile particles occur on the (0 1 1) and (1 1 0) faces, respectively [23]. Therefore, the presence of well-developed faces on TiO_2 particles is favorable to providing both oxidation and reduction sites. Moreover, it is expected that the efficiency of electron–hole separation is enhanced because of the difference in the electronic band structure between different crystal surfaces. Fig. 7 shows TEM and SEM images of rutile TiO_2 showing Pt deposits (a) and showing PbO_2 deposits (c) which were loaded on the particles of Pt/TiO_2. The deposited metals were analyzed by EDX (Fig. 7b and d). Fig. 7e shows SEM images of rutile TiO_2 particles showing PbO_2 deposits, which were loaded on the particles by UV irradiation of the Pt-deposited TiO_2 powder. Pt particles were deposited only on the (1 1 0) face as shown in Fig. 7a and b. This result indicates that the reduction site of rutile TiO_2 particles exists on the (1 1 0) face. Fig. 7c, d and e shows that the PbO_2 particles were deposited on the (1 1 1) faces. This means that the (1 1 1) face provides the oxidation site for rutile particles. The results shown in Fig. 7 indicate that the oxidation site and the reduction site on the rutile particles are on the (1 1 1) face and on the (1 1 0) face, respectively. Our results suggest that the (1 1 0) face of rutile particles provides an effective reduction site and that the (1 1 1) face works as the oxidation site. Because of the synergistic effect between the (1 1 0) and (1 1 1) faces, rutile particles are considered to be very efficient for some kinds of photocatalytic reactions.

Different surface energy levels of the conduction and valence bands are expected for different crystal faces of TiO_2 because of the atomic arrangements characteristic of these faces. The difference in the energy levels drives the electrons and holes to different crystal faces, leading to separation of electrons and holes [23]. The effective separation of oxidation and reduction sites of rutile particles, as shown in Fig. 7, suggests that the electronic energy levels of the (1 1 0) face are lower than those of the (1 1 1) face [22]. Ohno et al. suggested that the isolation of oxidation or reduction site on the surface of TiO_2 particles is large enough to drive the photocatalytic oxidation of water on rutile particles when suitable electron acceptors are added to the solution [23]. The effective separation of oxidation and reduction sites on the surface of rutile TiO_2 particles should be an important factor in obtaining the high efficiency of photocatalytic reactions.

4. Conclusion

A systematic approach was applied to the hydrothermal synthesis of rutile TiO_2 nanorods to gain an insight into the fundamental factors controlling particle size, crystal phase, crystal shape, and photocatalytic activity. The hydrothermal treatment resulted in the rutile TiO_2 nanorods being well-crystallized and well-dispersed without formation of large aggregates. The morphology of rutile crystals corresponds to faceted and elongated triangle-shaped particles. The particle size can be controlled by changing the experimental conditions and varies between 60 and 100 nm for rutile.

Well-crystallized nanosize rutile TiO_2 possessed higher levels of acetone and CO_2 evolution activity than those of MT-600B and ST-01 under UV light irradiation. It has been found that the photocatalytic activity increases with an increase in crystallite size. This suggests that electron–hole pair recombination plays an important role during the photodegradation of acetaldehyde and 2-propanol, at least under the present experimental conditions. Recombination is apparently slower in well-faceted and large rutile nanorods, thus increasing the activity, despite a decrease in the specific surface area. The degradation rate, higher than that of the most common reference material ST-01 and MT-600B, observed for faceted, well-dispersed, and relatively large triangle-shaped rutile crystals results from the combination of three factors: (i) an increase in photocatalytic activity with an increase in particle size, (ii) a high aspect ratio of the rutile crystals, and (iii) control of exposed crystal faces.

Acknowledgements

This work was partly supported by a grant of Knowledge of Cluster Initiative implemented by the Ministry of Education, Culture, Sports, Science and Technology (MEXT).

Appendix A. Supplementary data

Supplementary data associated with this article can be found, in the online version, at doi:10.1016/j.molcata.2008.10.048.

References

[1] M.R. Hoffmann, S.T. Martin, W. Choi, D.W. Bahnemann, Chem. Rev. 95 (1995) 69–96.
[2] Z. Zou, J. Ye, K. Sayama, H. Arakawa, Nature 414 (2001) 625–627.
[3] K. Kalyanasundaram, Coord. Chem. Rev. 46 (1982) 159–244.
[4] D.F. Ollis, H. Al-Ekabi, Photocatalytic Purification and Treatment of Water and Air, Elsevier, Amsterdam, 1993.
[5] W. Choi, Catal. Surv. Asia 10 (2006) 16–28.
[6] S. Cassaignon, M. Koelsch, J.-P. Jolivet, J. Phys. Chem. Solids 68 (2007) 695–700.
[7] E. Hosono, S. Fujihara, K. Kakiuchi, H. Imai, J. Am. Chem. Soc. 126 (2004) 7790–7791.
[8] X. Chen, S.S. Mao, Chem. Rev. 107 (2007) 2891–2959.
[9] N.R. Neale, A.J. Frank, J. Mater. Chem. 17 (2007) 3216–3221.
[10] X. Huang, C. Pan, J. Crystal Growth 306 (2007) 117–122.
[11] S. Watson, D. Beydonn, J. Scott, R. Amal, J. Nanopart. Res. 6 (2004) 193–207.
[12] H. Yin, Y. Wada, T. Kitamura, S. Kambe, S. Murasawa, H. Mori, T. Sakata, S. Yanagida, J. Mater. Chem. 11 (2001) 1694–1703.
[13] H. Cheng, J. Ma, Z. Zhao, L. Qi, Chem. Mater. 7 (1995) 663–671.
[14] J. Wei, J. Yao, X. Zhang, W. Zhu, H. Wang, M.J. Rhodes, Mater. Lett. 61 (2007) 4610–4613.
[15] K. Nagaveni, G. Sivalingam, M.S. Hegde, G. Mardras, Appl. Catal. B 48 (2004) 83–93.
[16] A.C. Jones, P.R. Chalker, J. Phys. D: Appl. Phys. 36 (2003) R80–R95.
[17] W.-N. Wang, I.W. Lenggoro, Y. Teashi, T.O. Kim, K. Okuyama, Mater. Sci. Eng. B 123 (2005) 194–202.
[18] K. Kakiuchi, E. Hosono, H. Imai, T. Kimura, S. Fujihara, J. Cryst. Growth 293 (2006) 541–545.
[19] C.A. Emilio, M.I. Litter, M. Kunst, M. Bouchard, C. Colbeau-Justin, Langmuir 22 (2006) 3606–3613.
[20] A. Testino, I.R. Bellobono, V. Buscaglia, C. Canevali, M. D'Arienzo, S. Polizzi, R. Scotti, F. Morazzoni, J. Am. Chem. Soc. 129 (2007) 3564–3575.
[21] T. Taguchi, Y. Saito, K. Sarukawa, T. Ohno, M. Matsumura, New J. Chem. 27 (2003) 1304–1306.
[22] P.M. Oliver, G.W. Watson, E.T. Kelsey, S.C. Parker, J. Mater. Sci. 7 (1997) 563–568.
[23] T. Ohno, K. Sarukawa, M. Matsumura, New J. Chem. 26 (2002) 1167–1170.
[24] Y. Matsumoto, M. Noguchi, T. Matsunaga, J. Phys. Chem. B 103 (1999) 7190–7194.
[25] C. Ribeiro, C. Vila, D.B. Stroppa, V.R. Mastelaro, J. Bettini, E. Longo, E.R. Leite, J. Phys. Chem. C 111 (2007) 5871–5875.
[26] K. Nishijima, B. Ohtani, X. Yan, T.-a. Kamai, T. Chiyoya, T. Tsubota, N. Murakami, T. Ohno, Chem. Phys. 339 (2007) 64–72.
[27] Y. Ohko, D.A. Tryk, K. Hashimoto, A. Fujishima, J. Phys. Chem. B 102 (1998) 2699–2704.
[28] A. Fujishima, T.N. Rao, D.A. Tryk, J. Photochem. Photobiol. C 1 (2000) 1–21.
[29] N.J. Peill, M.R. Hoffmann, Environ. Sci. Technol. 32 (1998) 398–404.
[30] L. Yang, Z. Liu, J. Shi, Y. Zhang, H. Hu, W. Shangguan, Sep. Purif. Technol. 54 (2007) 204–211.